A Flexible Bidirectional Fiber-FSO-5G Wireless Convergent System

Chung-Yi Li [ID], Hai-Han Lu [ID], *Senior Member, IEEE*, Cing-Ru Chou [ID], Hsin-Mao Hsia, Chao-Yu Feng [ID], Yi-Hao Chen, Yu-Ting Huang, and Agustina Nainggolan [ID]

Abstract—A flexible bidirectional fiber-free-space optical (FSO)-fifth-generation (5G) wireless convergent system with 1-Gb/s/4.5-GHz sub-6 GHz and 10-Gb/s/28-GHz millimeter-wave (MMW) (downstream), as well as 10-Gb/s/24-GHz MMW (upstream) 5G hybrid data signals is built, employing a vertical cavity surface emitting laser (VCSEL)-based wavelength selector and a remotely injection-locked distributed feedback laser diode (DFB LD) for presentation. It is the first to adopt a VCSEL-based wavelength selector to adaptively provide 5G applications and an injection-locked DFB LD to perform a phase modulation-to-intensity modulation transformation with an optical-to-electrical conversion. Good bit error rate performance and acceptable eye diagrams are achieved over 25 km single-mode fiber transport, 600 m FSO link, and 10 m/4 m RF wireless transmission. Such demonstrated fiber-FSO-5G wireless convergent system is a promising one toward optical-based long-haul networks at comparatively high-speed operations. It exhibits an excellent convergence not only due to its development for incorporating optical fiber with optical/5G wireless networks, but also due to its enhancement for flexible two-way high-speed and long-haul communications.

Index Terms—Fiber-FSO-5G wireless convergence, fifth-generation (5G), VCSEL-based wavelength selector, remotely injection-locked DFB LD.

I. INTRODUCTION

IN recent decades, plentiful innovations in mobile telecommunications and its incorporation with optical communications have greatly pushed industrial revolutions. Broadband access networks are developing on the advantages of both optical and wireless technologies to realize fiber-free-space optical (FSO)-fifth-generation (5G) wireless convergences, which increase the transmission capacity and enhance the coverage area. 5G networks make use of prolifically innovative and

developing technologies to provide a variety of emerging applications, such as high-speed Internet, 4K/8K ultra-HD video streaming, autonomous vehicles, smart homes/cities, Internet of Things, etc. [1]–[8]. However, the 5G signal has less ability to transport wirelessly because of its low diffraction trait. Affording broadband heterogeneous services with high-transmission-rate and long-reach transmission is critically important. FSO communications, which deliver optical signals by laser beam propagation in free space, have received much attention for resolving the problem of short-reach 5G wireless transmission [9]–[12]. FSO-5G wireless convergences can greatly reduce the number of 5G base stations (BSs). Given the advancements in 5G and FSO technologies, FSO-5G wireless convergences have been developed to provide multi-gigabit services through the long-reach free-space link with short-reach RF wireless transmission [13]–[16]. Additionally, given the fast enhancement of lightwave transmission systems, increasing demands drive the requirements for high-speed and long-haul applications, not only for the backbone network based on single-mode fiber (SMF), but also for the FSO-5G-based reach extender. As a high-bandwidth transmission medium, SMF offers exceptional transmission qualities with low attenuation coefficient. Obvious advantages are afforded by deploying the SMF to increase the transmission capacity and the coverage area of the FSO-5G wireless convergences at relatively high speed using the traits of optical fiber and optical/5G wireless communications. To incorporate fiber backbone with FSO-5G wireless convergences, fiber-FSO-5G wireless convergences hold the capabilities of high transmission capacity with long-haul transmission. Employing laser lights, sub-6 GHz, and millimeter-wave (MMW) carriers, a bidirectional fiber-FSO-5G wireless convergent system can be built to satisfy the targets of high-transmission-rate with long-haul transmission (as presented in Fig. 1).

In this work, a flexible bidirectional fiber-FSO-5G wireless convergent system is successfully demonstrated, with a dual-arm Mach-Zehnder modulator (MZM) to transport downstream intensity-modulated 1-Gb/s/4.5-GHz 5G sub-6 GHz and 10-Gb/s/28-GHz 5G MMW hybrid data signals, and a phase modulator to deliver an upstream phase-remodulated 10-Gb/s/24-GHz 5G MMW data signal. The high-frequency band in the spectrum above 24 GHz (MMW) is targeted to provide a high data rate of 10 Gb/s, whereas the low-frequency band in the spectrum below 6 GHz (sub-6 GHz) is targeted to afford a low data rate of 1 Gb/s. 5G MMW's limitations make it best suited for dense, urban areas, or specific areas such as train station or
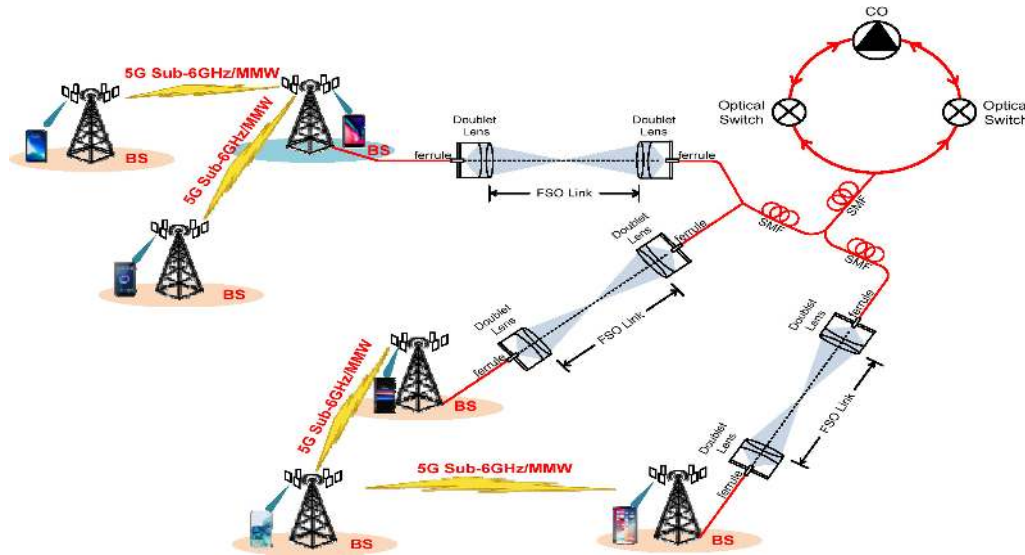
Fig. 1. A flexible bidirectional fiber-FSO-5G wireless convergence with high transmission capacity and long-haul transmission traits.

airport. In rural and suburban areas, 5G MMW technology is not practical because it doesn't have enough range which is where the 5G sub-6 GHz networks come in. This proposed flexible bidirectional fiber-FSO-5G wireless convergent system can not only provide 5G MMW applications for dense/urban and specific areas, but it can also provide 5G sub-6 GHz applications for rural and suburban areas. It reveals a prominent one for 5G applications to target the urban/specific area with high data rate and the rural/suburban area with low data rate. For downlink transmission, a fiber-FSO-5G wireless convergence with 1-Gb/s/4.5-GHz sub-6 GHz and 10-Gb/s/28-GHz MMW 5G hybrid data signals over 25 km SMF transport, 600 m FSO link, and 10 m/4 m RF wireless transmission is practically constructed. With the adoption of a wavelength selector based on a vertical cavity surface emitting laser (VCSEL), one of the intensity-modulated optical signals is adaptively chosen. By varying the VCSEL's operating current, the wavelengths selected by a VCSEL-based wavelength selector can be varied to adaptively choose the optical signal [17], [18]. As central optical carrier and +1 optical sideband spaced by 4.5 GHz are selected, a 1-Gb/s/4.5-GHz 5G sub-6 GHz data signal is produced. Further, as central optical carrier and +1 optical sideband spaced by 28 GHz are picked, a 10-Gb/s/28-GHz 5G MMW data signal is generated. With a VCSEL-based wavelength selector, the optical signal is adaptively chosen for 5G sub-6 GHz or MMW application. To the author's knowledge, this is the first to build a high-speed and long-haul fiber-FSO-5G wireless convergence with a VCSEL-based wavelength selector to flexibly provide 5G certain services and applications. This proposed fiber-FSO-5G wireless convergence is attractive because it prevents the requirements of several optical band-pass/band-rejection filters [19], sophisticated micro-electromechanical systems-based wavelength selector [20], and elaborate liquid crystal-based wavelength selector [21]. The system exhibits notable the benefits of simplicity and flexibility. For uplink transmission, an FSO-fiber-5G wireless convergence with 10-Gb/s/24-GHz 5G MMW data signal

over a 600-m FSO link, 25-km SMF transport, and 4-m RF wireless transmission is practically built. A distributed feedback laser diode (DFB LD) with remote injection locking is employed to transform a phase-modulated 10-Gb/s/24-GHz 5G MMW optical signal into an intensity-modulated one and to operate an optical-to-electrical (O/E) conversion. A remotely injection-locked DFB LD works effectively as a transformer for phase modulation (PM)-to-intensity modulation (IM) and an optical detector. Given the proposed upstream FSO-fiber-5G wireless convergence does not use an elaborate fiber Bragg grating tilt filter [22] or a sophisticated Brillouin-assisted carrier phase shift [23] for PM-to-IM transformation, it discloses a promising convergence with low-complexity advantage. The performances of downstream 1-Gb/s/4.5-GHz 5G sub-6 GHz and 10-Gb/s/28-GHz 5G MMW data signals, as well as upstream 10-Gb/s/24-GHz 5G MMW data signal are evaluated by bit error rate (BER) values and eye diagrams. Over 25 km SMF transport, 600 m FSO link, and 10 m/4 m RF wireless transmission, high BER performance and qualified eye diagrams are attained to fully satisfy the demands of 5G communications.

A flexible bidirectional fiber-FSO-5G wireless convergent system with 1-Gb/s/4.5-GHz (sub-6 GHz), 10-Gb/s/24-GHz (MMW), and 10-Gb/s/28-GHz (MMW) 5G hybrid data signals is successfully constructed for the first time. For downstream modulation, the practicality of delivering 4.5 GHz sub-6 GHz and 28 GHz MMW 5G hybrid data signals with a VCSEL-based wavelength selector to adaptively afford the desired 5G application is feasibly developed. For upstream modulation, the practicality of delivering 24 GHz 5G MMW data signal with a remotely injection-locked DFB LD to carry out a PM-to-IM transformation and an O/E conversion is successfully made. Such proposed fiber-FSO-5G wireless convergence is an innovation aimed at implementing optical-based long-haul networks with relatively high-speed operations. It presents a noteworthy convergence not only due to its progression for incorporating optical fiber with optical/5G wireless networks, but also

due to its development for two-way high-speed and long-haul transmissions.

II. EXPERIMENTAL SETUP

Fig. 2 presents the configuration of the demonstrated flexible bidirectional fiber-FSO-5G wireless convergent system with a dual-arm MZM to deliver downstream intensity-modulated 1-Gb/s/4.5-GHz sub-6 GHz and 10-Gb/s/28-GHz MMW 5G hybrid data signals, and a phase modulator to transmit an upstream phase-remodulated 10-Gb/s/24-GHz 5G MMW data signal. After polarization using a polarization controller (PC1), DFB LD1, with a central wavelength of 1540.62 nm (λ_1), applies an optical carrier on the dual-arm MZM (Sumitomo T.DEH1.5-40). A 1-Gb/s non-return-to-zero (NRZ) data stream mixes with a 4.5-GHz MW carrier to create a 1-Gb/s/4.5-GHz 5G sub-6 GHz data signal. After traveling through a modulator driver, this 1-Gb/s/4.5-GHz 5G sub-6 GHz data signal drives one arm of the dual-arm MZM. Further, a 10-Gb/s NRZ data stream mixes with a 28-GHz MMW carrier to produce a 10-Gb/s/28-GHz 5G MMW data signal. After passing through a modulator driver, this 10-Gb/s/28-GHz MMW data signal drives the other arm of the dual-arm MZM. Here, we electrically mix the data and the carrier before modulating the optical modulator. Given that appropriate 5G sub-6 GHz and MMW hybrid data signals are supplied in the dual-arm MZM, only the first-order sidebands are produced, with wavelength spacing of 4.5 GHz (0.036 nm) and 28 GHz (0.224 nm). After polarization using a PC2, the 1-Gb/s/4.5-GHz sub-6 GHz and 10-Gb/s/28-GHz MMW hybrid data signals are boosted by an erbium-doped fiber amplifier (EDFA), adjusted by a variable optical attenuator (VOA), circulated by an optical circulator (OC1), and communicated over 25 km SMF link. A VOA in front of 25 km SMF optimizes the optical power supplied in the 25 km fiber links to acquire the best transmission performances. After that, the optical signal is transported through 600 m FSO link using a couple of doublet lenses. Laser light's free-space distance is increased to 600 m (50 m × 12) by adopting multiple plane mirrors on both sides [24].

Through an optical wired-wireless link of 25.6 km (25 km SMF + 600 m free-space), the optical signals are circulated by an OC2 and then supplied in a wavelength selector based on a VCSEL to adaptively choose one of the optical signals. This VCSEL-based wavelength selector is composed of one OC, one PC, and one VCSEL. Given that VCSEL's wavelength shift with the temperature variation is 0.02 nm/°C, a temperature controller is employed in the VCSEL-based wavelength selector to overcome wavelength shift problem due to temperature variation. For upper path, a 1-Gb/s/4.5-GHz 5G sub-6 GHz data signal is adaptively chosen by the wavelength selector. Fig. 3(a) [inset (a) of Fig. 2] shows the optical spectrum before passing through the wavelength selector. An injection locking increases lower sideband's intensity and produces the optical spectrum as illustrated in Fig. 3(b) [inset (b) of Fig. 2]. The 1-Gb/s/4.5-GHz sub-6 GHz data signal is next detected by a 5-GHz photodiode (PD) (Thorlabs DET08CFC), amplified by a power amplifier (PA) with 4.4-5.0 GHz frequency range (Qorvo

QPA4501), and wirelessly transmitted by a set of 4.5-GHz BS antennas (MTI MT-443008). After a 10-m RF wireless link, the 1-Gb/s/4.5-GHz sub-6 GHz data signal is detected by an envelope detector (ED) with 0.5-43.5 GHz frequency range (Analog Devices ADL6010), and driven by a wideband low-noise (LN) driver with DC-40 GHz frequency range (Anritsu AH34152A). After driving, the 1-Gb/s NRZ data stream is applied to a BER tester (BERT) (Anritsu MP1900A) to measure the BER values. Additionally, a digital storage oscilloscope (DSO) (Keysight N1000A DCA-X) is deployed to catch the eye diagrams of 1 Gb/s NRZ data stream. For middle path, a 10-Gb/s/28-GHz 5G MMW data signal is adaptively selected by the wavelength selector. An injection locking boosts lower sideband's intensity and yields the optical spectrum as displayed in Fig. 3(c) [inset (c) of Fig. 2]. Then, the 10-Gb/s/28-GHz MMW data signal is received by a 30-GHz PD (Optilab PR-30-A), boosted by a PA with 27-31 GHz frequency range (Qorvo TGA2594-HM), and wirelessly transmitted by a pair of Ka-band horn antennas (HAs) (Warison WGAT-26.5-40). After a 4-m RF wireless transport, the 10-Gb/s/28-GHz MMW data signal is detected by an ED and driven by a wideband LN driver. Afterward, the 10-Gb/s NRZ data stream is sent to a BERT for BER performance analysis. Furthermore, a DSO is used to capture the eye diagrams of 10 Gb/s NRZ data stream. For lower path, a central carrier is adaptively picked by the wavelength selector. An injection locking intensifies central carrier's intensity and yields the optical spectrum as displayed in Fig. 3(d) [inset (d) of Fig. 2]. Afterward, the enhanced central carrier is reused and remodulated by a phase modulator (Thorlabs LN66S) for upstream modulation.

For upstream modulation, a 10-Gb/s/24-GHz 5G MMW data signal goes through a modulator driver and then supplies in a phase modulator. The upstream optical signal is boosted by an EDFA, optimized by a VOA, circulated by an OC2, and communicated through 600-m free-space transmission with 25 km SMF transport. Next, the upstream optical signal is circulated by an OC1 and injected into a DFB LD2 (λ_c = 1540.40 nm) to make a PM-to-IM transformation and an O/E conversion. The optical spectrum before remote injection locking is exhibited in Fig. 4(a) [inset (i) of Fig. 2]. Remote injection locking increases the upper sideband's intensity and produces the optical spectrum as expected in Fig. 4(b) [25], [26]. Then, the 10-Gb/s/24-GHz 5G MMW data signal is amplified by a PA with 17-24 GHz frequency range (Qorvo TGA2522-SM), and wirelessly delivered by a pair of K-band HAs (Warison WGAT-18-26.5). Through 4 m RF wireless link, the data signal is envelope-detected by an ED and enhanced by a LN driver. Moreover, the eye diagrams of 10 Gb/s NRZ data stream are captured by a DSO.

III. EXPERIMENTAL RESULTS AND DISCUSSIONS

Regarding the VCSEL-based wavelength selector, VCSEL's central wavelengths at different operating currents are listed in Table 1. It is to be found that as the VCSEL's operating current adjusts from 2.61 to 2.66 mA, the VCSEL's central wavelength varies from 1540.63 to 1540.85 nm. An adjusting range of 0.22 nm is attained to adaptively enhance the optical signal's central carrier or the +1 sideband. As the VCSEL's
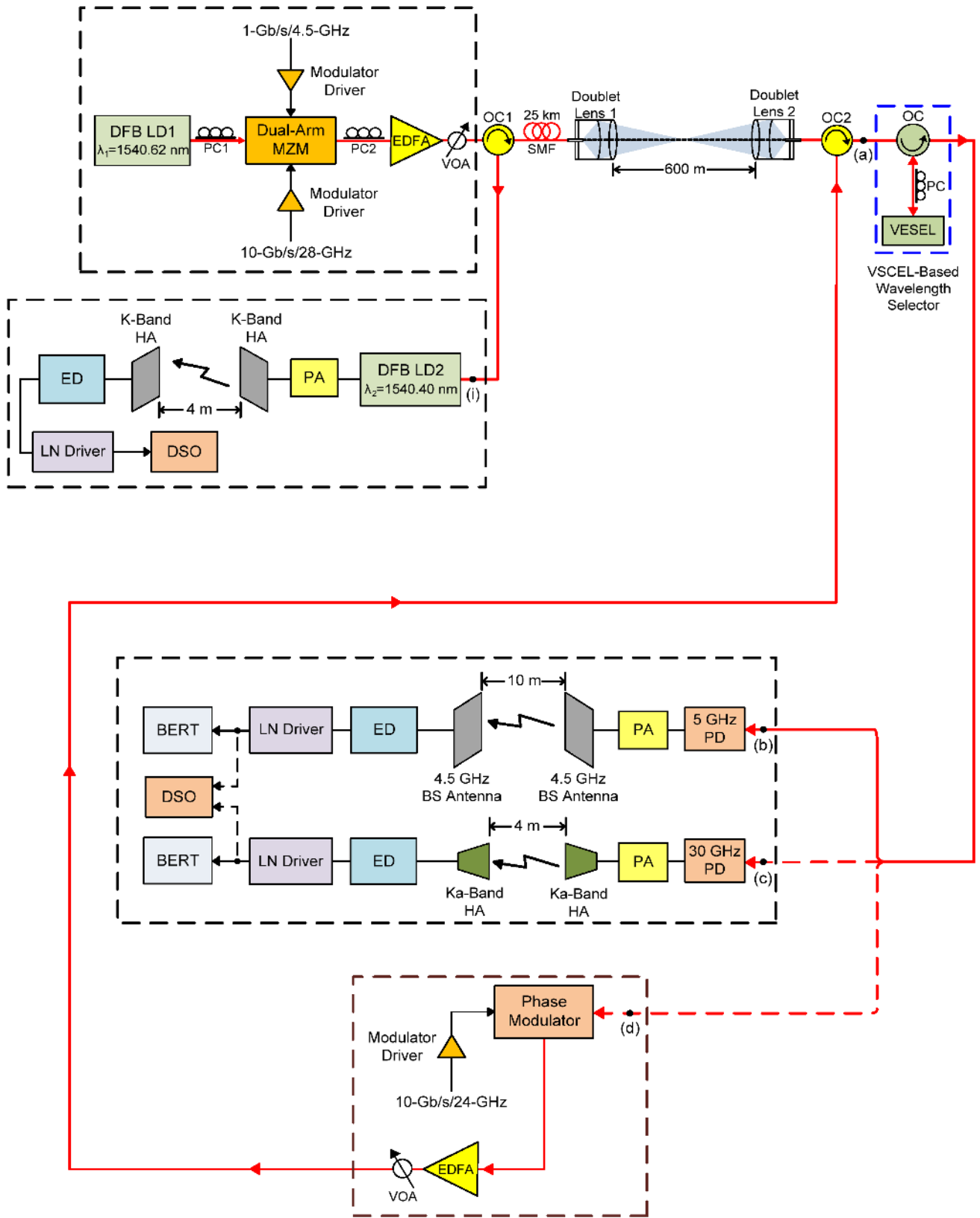
Fig. 2. Configuration of demonstrated flexible bidirectional fiber-FSO-5G wireless convergent system with a dual-arm MZM to deliver downstream intensity-modulated 1-Gb/s/4.5-GHz sub-6 GHz and 10-Gb/s/28-GHz MMW 5G hybrid data signals, and a phase modulator to transmit an upstream phase-remodulated 10-Gb/s/24-GHz 5G MMW data signal.
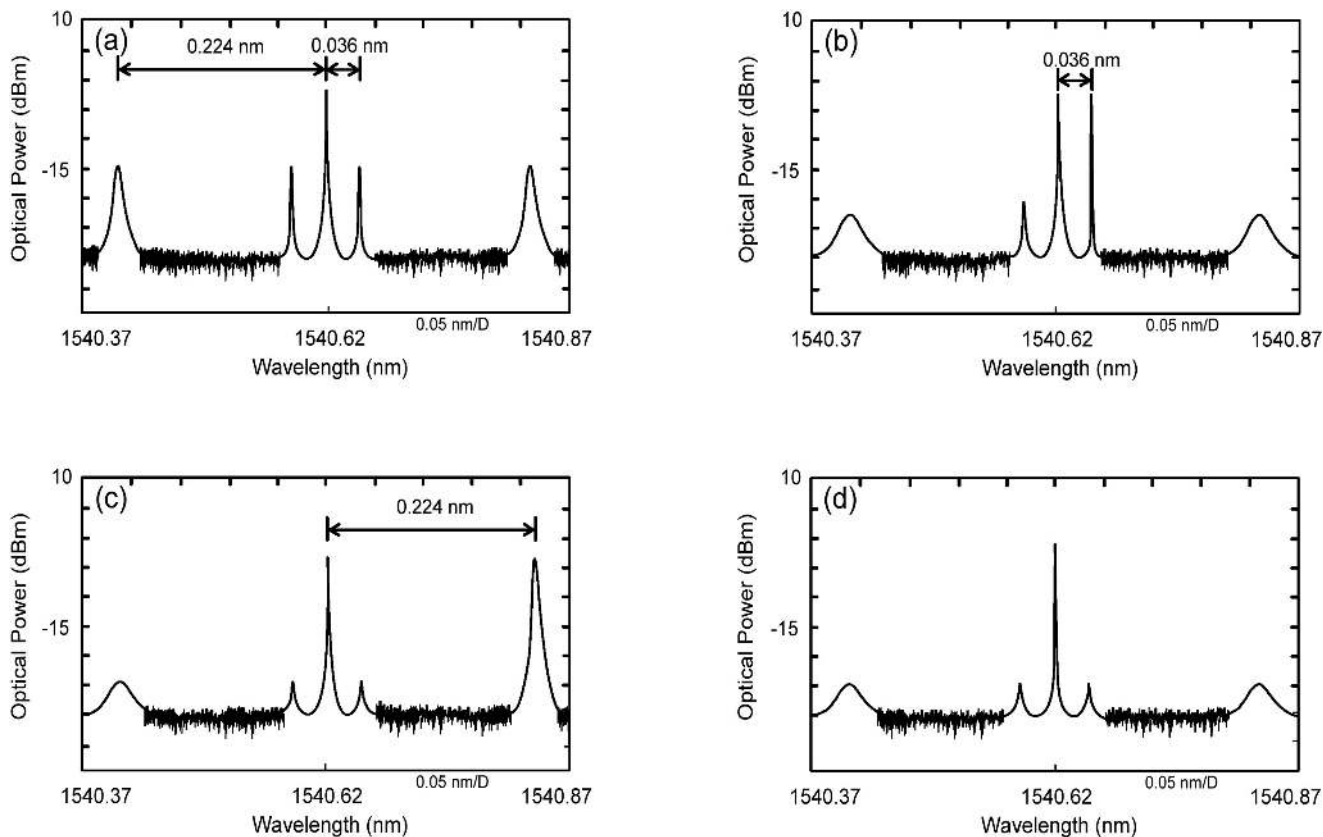
Fig. 3. (a) The optical spectrum before passing through the VCSEL-based wavelength selector. (b) Injection locking increases lower sideband's intensity (1-Gb/s/4.5-GHz 5G sub-6 GHz data signal). (c) Injection locking boots lower sideband's intensity (10-Gb/s/28-GHz 5G MMW data signal). (d) Injection locking enhances central carrier's intensity.
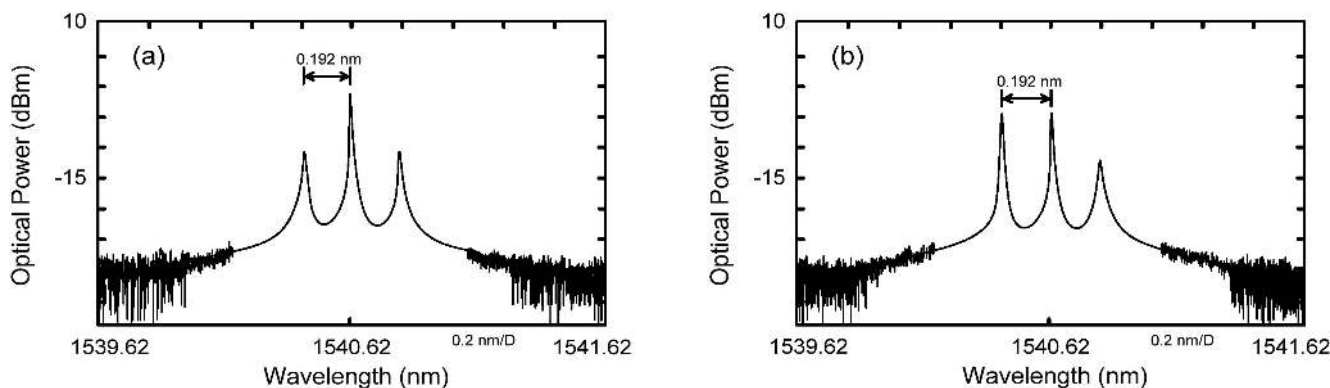
Fig. 4. (a) The optical spectrum before remote injection locking. (b) Remote injection locking enhances the upper sideband's intensity.

TABLE 1
VCSEL'S CENTRAL WAVELENGTHS AT DIFFERENT OPERATING CURRENTS

Operating Current (mA)	2.61	2.63	2.65	2.67	2.69	2.62	2.66
Central Wavelength (nm)	1540.63	1540.66	1540.71	1540.74	1540.78	1540.81	1540.85

TABLE 2
THE STATUS OF DFB LD2 WITH REMOTE INJECTION UNDER VARIOUS WAVELENGTH DETUNING ($\Delta\lambda = \lambda_1 - \lambda_2$), AND THE UPSTREAM MODULATION
RESPONSE IN THE STATES OF DFB LD2 WITH REMOTE INJECTION LOCKING AND SEVERE OSCILLATION

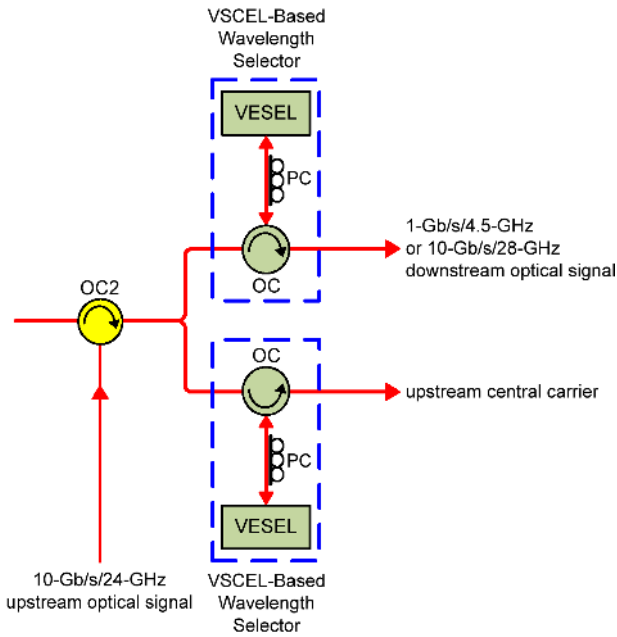| $\Delta\lambda = \lambda_1 - \lambda_2$ (nm)	0.42	0.32	0.22	0.12	0	− 0.12	− 0.22	− 0.32
Status	Severe Oscillation	Injection Locking	Injection Locking	Injection Locking	Injection Locking	Injection Locking	Injection Locking	Severe Oscillation
Upstream Modulation Response (GHz)	Noise	23.8	24.1	23.9	23.8	24.1	23.8	Noise

Fig. 5. Employing two VCSEL-based wavelength selectors in a bidirectional fiber-FSO-5G wireless convergent system.

central wavelength is 1540.63 nm, the central carrier is thus selected for uplink transmission. Substituting the LD for uplink transmission, the network operator can thereby flexibly construct a bidirectional fiber-FSO-5G wireless convergent system. Furthermore, as VCSEL's central wavelength moves toward 1540.66 nm, the 1-Gb/s/4.5-GHz optical signal is consequently selected for 5G sub-6 GHz application. Moreover, as the VCSEL's central wavelength moves further toward 1540.85 nm, the 10-Gb/s/28-GHz optical signal is accordingly chosen for 5G MMW application. By varying the VCSEL's operating current (central wavelength), the optical signal picked by the wavelength selector based on a VCSEL can be adjusted to adaptively afford 5G certain services and applications.

VCSEL-based wavelength selector can only choose one of the three optical signals (central carrier, 1-Gb/s/4.5-GHz or 10-Gb/s/28-GHz optical signal), the upstream optical carrier cannot coexist with the 1-Gb/s/4.5-GHz or 10-Gb/s/28-GHz downstream optical signal. When the 1-Gb/s/4.5-GHz or 10-Gb/s/28-GHz downstream optical signal is working, there is no upstream central carrier. To resolve this problem, two VCSEL-based wavelength selectors can be employed in the

bidirectional fiber-FSO-5G wireless convergent system (as illustrated in Fig. 5). One is utilized for selecting 1-Gb/s/4.5-GHz or 10-Gb/s/28-GHz downstream optical signal, and the other is utilized for producing upstream central carrier.

Table 2 shows the status of DFB LD2 with remote injection under various wavelength detuning ($\Delta\lambda = \lambda_1 - \lambda_2$). In the wavelength detuning range of −0.22 to 0.32 nm, an injection locking state exists. In the remote injection locking scenario, DFB LD2 works as a PM-to-IM transformer with an O/E converter. Not in the wavelength detuning range of −0.22 to 0.32 nm, nevertheless, a severe oscillation state occurs. Table 2 also shows the upstream modulation response in the states of DFB LD2 with remote injection locking and severe oscillation (non-injection locking). In the state of severe oscillation, noise and poor upstream modulation response are obtained. In the remote injection locking state, however, an enhanced upstream modulation response (>23.8 GHz) is attained. The results reveal that a remotely injection-locked DFB LD2 is powerful enough to simultaneously transform and detect an upstream 10-Gb/s/24-GHz 5G MMW data signal. In addition, it should be noted that optimal remote injection locking appears at a wavelength detuning of 0.22 or −0.12 nm. With optimal remote injection locking, a highest upstream modulation response of 24.1 GHz is achieved.

Fig. 6(a) exhibits the BER performances of 1-Gb/s/4.5-GHz 5G sub-6 GHz data signal in back-to-back (BTB) state, through 25 km SMF transport, through 25 km SMF transport with 600 m FSO link, as well as through 25 km SMF transport, 600 m FSO link, and 10 m RF wireless transmission. As BER is 10^{-9}, there is a large power penalty of 5.6 dB between BTB and that through 25 km SMF transport. This 5.6 dB power penalty arises chiefly from dispersion-induced distortion because of 25 km SMF transport. Over 25 km SMF transport, fiber dispersion deteriorates the transmission quality and produces worse BER. Further, with a 10^{-9} BER operation, a low power penalty of 1.6 dB appears between the states through 25 km SMF transport and through 25 km SMF transport with 600 m FSO link. This 1.6 dB low power penalty is mainly ascribed to the atmospheric attenuation from the 600-m free-space transmission. Through 600-m FSO link, the atmospheric attenuation fluctuates from 1.2 dB (sunny weather) to 50 dB (heavy rain/snow/fog weather) [27]–[30]. Here, an atmospheric attenuation of approximately 1.6 dB exists owing to the 600-m free-space transmission. In addition, as BER is 10^{-9}, a power penalty of 1.8 dB is observed between the scenario through 25 km SMF transport with 600 m
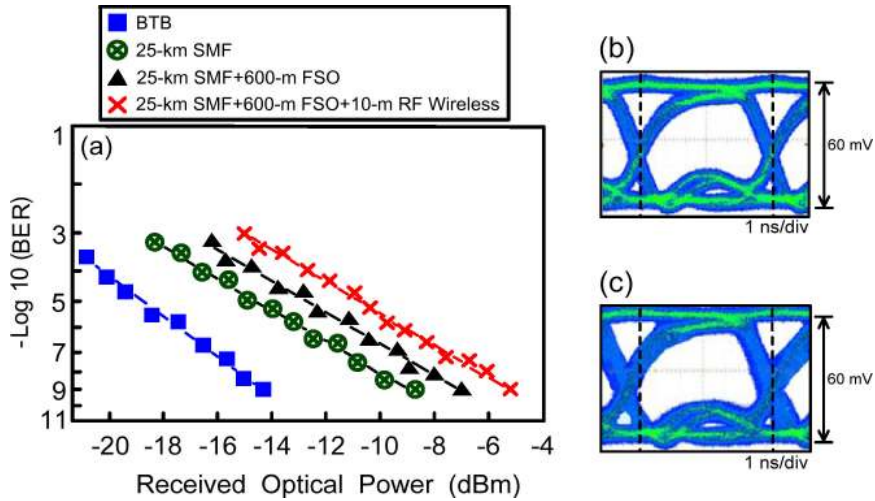
Fig. 6   (a) BER performances of 1-Gb/s/4.5-GHz 5G sub-6 GHz data signal in various states. The eye diagrams of 1-Gb/s/4.5-GHz data signal in the states (b) through 25 km SMF transport, and (c) through 25 km SMF transport, 600 m FSO link, and 10 m RF wireless transmission.
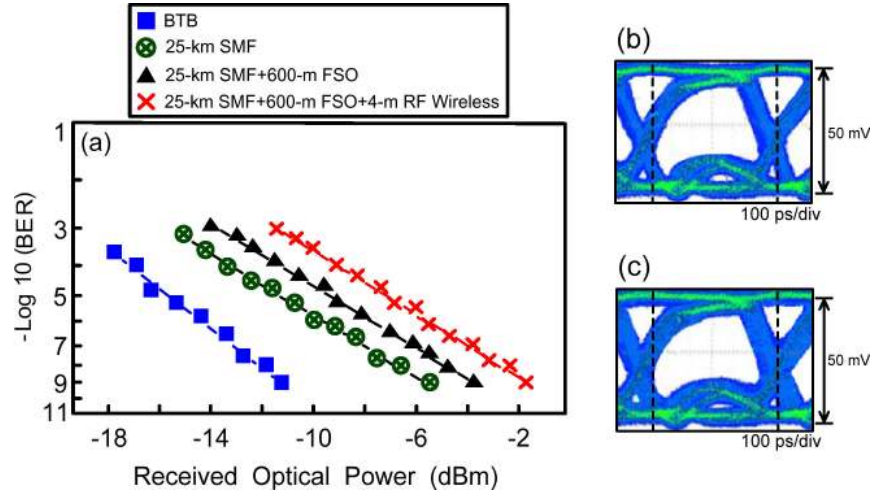

Fig. 7   (a) BER performances of 10-Gb/s/28-GHz 5G MMW data signal under different scenarios. The eye diagrams of 10-Gb/s/28-GHz data signal in the scenarios (b) over 25 km SMF transport, and that (c) over 25 km SMF transport, 600 m FSO link, and 4 m RF wireless transmission.

FSO link and that through 25 km SMF transport, 600 m FSO link, and 10 m RF wireless transmission. Over 10 m RF wireless transmission, 1-Gb/s/4.5-GHz 5G sub-6 GHz data signal experiences fading, thereby causing received signal's amplitude and phase fluctuations and bringing on reduced BER. As for eye diagrams, Figs. 6(b) and 6(c) display the eye diagrams of 1-Gb/s/4.5-GHz data signal in the states through 25 km SMF transport, and through 25 km SMF transport, 600 m FSO link, and 10 m RF wireless transmission. Through 25 km SMF transport, open eye diagrams are captured at a received optical power of -8.7 dBm and a BER of 10^{-9} [Fig. 6(b)]. In the state through 25 km SMF transport, 600 m FSO link, and 10 m RF wireless transmission, clear eye diagrams are captured at a received optical power of -5.3 dBm and a BER of 10^{-9} [Fig. 6(c)].

Fig. 7(a) presents the BER performances of 10-Gb/s/28-GHz 5G MMW data signal under different scenarios. With a 10^{-9} BER operation, power penalties of 5.8 dB, 1.6 dB, and 2 dB

exist among BTB, over 25 km SMF transport, over 25 km SMF transport with 600 m FSO link, and over 25 km SMF transport, 600 m FSO link with 4 m RF wireless transmission. A 5.8-dB power penalty is primarily ascribed to the fiber dispersion introduced by the 25 km SMF transmission, a 1.6-dB power penalty is mostly arisen from the atmospheric attenuation on account of the 600 m free-space transmission, and a 2-dB power penalty is mostly attributed to the fading effect from the 4 m RF wireless transmission [31]–[33]. Power penalty due to fiber dispersion (PP_D) is given by [34]:

$$PP_D = 10 log \left[1 + 0.5 \left(\frac{F_R}{F_L} \right)^2 \right] \qquad (1)$$

where F_R is the received data rate, and F_L is the bandwidth-distance product. According to the above equation, the power penalty difference due to 25 km SMF transmission between
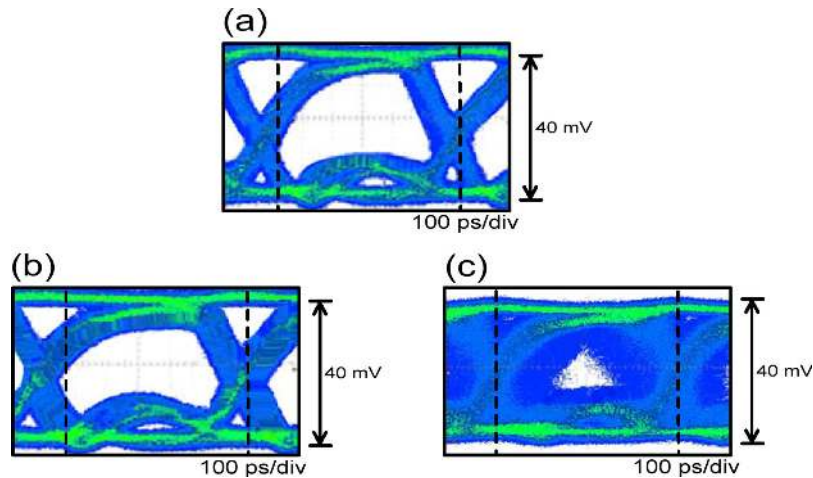
Fig. 8. Eye diagrams of upstream 10-Gb/s/24-GHz 5G MMW data signal in the conditions of (a) 0.22 nm wavelength detuning with 3 dBm injection, (b) 0.22 nm wavelength detuning with −3 dBm injection, and (c) 0.42 nm wavelength detuning.

10-Gb/s/28-GHz 5G MMW data signal and 1-Gb/s/4.5-GHz 5G sub-6 GHz data signal is approached to 0 dB ($10 \log[1 + 0.5(\frac{10}{28 \times 25})^2] - 10 \log[1 + 0.5(\frac{1}{4.5 \times 25})^2] \sim 0$), which almost corresponds with the experimental power penalty difference of 0.2 dB (5.8 − 5.6 = 0.2). Moreover, provided that higher data rate needs higher received optical power to compensate for the optical signal-to-noise ratio penalty [35], the received optical power of the 10-Gb/s/28-GHz MMW optical signal [Fig. 7(a)] is thereby around 3.3 dB higher than that of the 1-Gb/s/4.5-GHz sub-6 GHz optical signal [Fig. 6(a)]. Regarding eye diagrams, in the scenario over 25 km SMF transport, clear eye diagrams [Fig. 7(b)] are captured at a received optical power of −5.4 dBm and a BER of 10^{-9}. In the scenario over 25 km SMF transport, 600 m FSO link, and 4 m RF wireless transmission, somewhat clear eye diagrams [Fig. 7(c)] are yielded at a received optical power of −1.8 dBm and a BER of 10^{-9}.

Figs. 8(a), 8(b), and 8(c) exhibit the eye diagrams of upstream 10-Gb/s/24-GHz 5G MMW data signal in the respective conditions of 0.22 nm wavelength detuning with 3 dBm injection, 0.22 nm wavelength detuning with −3 dBm injection, and 0.42 nm wavelength detuning. With a wavelength detuning of 0.22 nm and an injection power of 3 dBm, clear eye diagrams [Fig. 8(a)] are captured. With a wavelength detuning of 0.22 nm and an injection power of −3 dBm, somewhat clear eye diagrams [Fig. 8(b)] are acquired. Over 600 m FSO link, 25 km SMF transport, and 4 m RF wireless transmission, results show that a remotely injection-locked DFB LD can practically transform and detect the transmitted 10-Gb/s/24-GHz data signal. As the PM-to-IM transformation and detection efficiencies of the remotely injection-locked DFB LD are proportional to the injection power level [36], a remote injection locking with higher injection power level produces higher transformation and detection efficiencies, and thereby enhances the eye diagram's quality. Moreover, it is to be found that an amplitude penalty of around 10 mV emerges between Fig. 7(c) and Fig. 8(a). Given that a 30-GHz PD has a higher responsivity than that of an optimally injection-locked DFB LD2 with 24.1 GHz bandwidth [37], the eye diagram amplitude of the Fig. 8(a) is thus degraded by about 10 mV, compared to that of Fig. 7(c). Whereas for

a wavelength detuning of 0.42 nm, eye diagram's fluctuations are obviously observed in Fig. 8(c). DFB LD2 is ineffectively injection-locked because 0.42 nm is not in the wavelength detuning range of −0.22 to 0.32 nm, which caused considerable fluctuations in the eye diagram. Additionally, it is to be noted that the eye diagrams in Figs. 6(b), [6(c)], [7(b)], [7(c)], [8(a)], and [8(b)] have the same distortion in the lower eyelid, which results in somewhat vertical eye closure. However, the area between the higher eyelid and the lower eyelid still meets the demand of open/clear eye diagrams. The distortion in the lower eyelid is mostly attributed to the optical impedance mismatching [38]. However, it can be mitigated by providing a smooth transmission to minimize light loss due to reflection at the interface.

The 5G new radio standard uses orthogonal frequency-division multiplexing (OFDM) on both the downlink and uplink transmissions. The subcarrier modulation can be quadrature phase shift keying (QPSK), 16-quadrature amplitude modulation (QAM), 64-QAM or 256-QAM. To have more association with the 5G physical layer and this flexible bidirectional fiber-FSO-5G wireless convergent system, 1-Gb/s/4.5-GHz and 10-Gb/s/28-GHz 16-QAM-OFDM data signals are utilized to drive the dual-arm MZM (downstream modulation), and 10-Gb/s/24-GHz 16-QAM-OFDM data signal is utilized to drive the phase modulator (upstream modulation). These 16-QAM-OFDM data signals are generated offline by MATLAB programs and uploaded into Tektronix arbitrary waveform generators (two AWG70001 + one AWG7102). Through 25 km SMF transport, 600 m FSO link, and 10 m (4 m) RF wireless transmission (downlink), 1-Gb/s/4.5-GHz (10-Gb/s/28-GHz) 16-QAM-OFDM data signal is captured by a communication signal analyzer and post-processed by MATLAB program to calculate the BER value and the corresponding constellation map. Over 600 m FSO link, 25 km SMF transport, and 4 m RF wireless transmission (uplink), in the scenario of 0.22 nm wavelength detuning with 3 dBm injection, 10-Gb/s/24-GHz 16-QAM-OFDM data signal is seized by a communication signal analyzer and post-processed by MATLAB program to calculate the BER value and the related constellation map. Figs. 9(a), [9(b), and [9(c) show the BER values and the constellation maps of the 1-Gb/s/4.5-GHz,
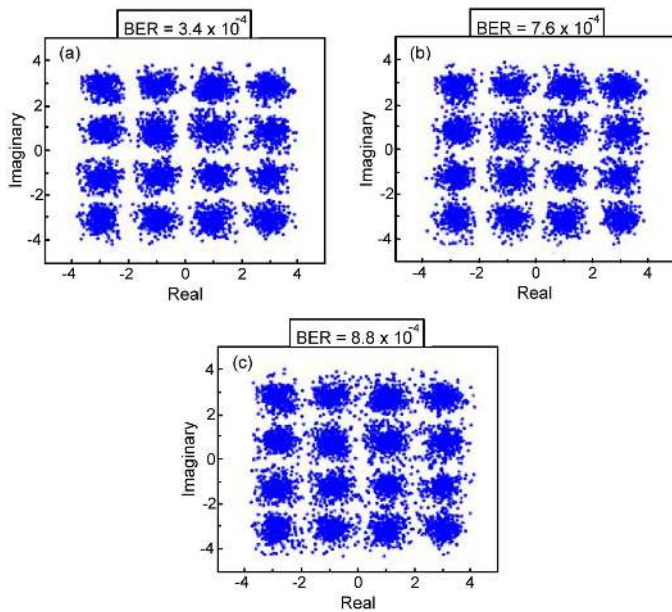
Fig. 9. The BER values and the constellation maps of (a) 1-Gb/s/4.5-GHz, (b) 10-Gb/s/28-GHz, and (c) 10-Gb/s/24-GHz 16-QAM-OFDM data signals after downlink/uplink transmission.

10-Gb/s/28-GHz, and 10-Gb/s/24-GHz 16-QAM-OFDM data signals, respectively, after downlink/uplink transmission. For downlink transmission, BER values of 3.4×10^{-4} [Fig. 9(a)] and 7.6×10^{-4} [Fig. 9(b)] with clear constellation maps are attained. For uplink transmission, BER value of 8.8×10^{-4} and a slight clear constellation map are achieved [Fig. 9(c)]. BER values reach 10^{-4} order of magnitude, which are well below the forward error correction limit criterion of 3.8×10^{-3}. Sufficiently low BER values and clear constellation maps demonstrate the feasibility of building a flexible bidirectional fiber-FSO-5G wireless convergent system. For a flexible bidirectional fiber-FSO-5G wireless convergent system, the modulation formats are digital modulations such as on-off keying (OOK), QPSK, 16-QAM-OFDM, and 64-QAM-OFDM. In the proof-of-concept experiment, OOK is applied to the flexible bidirectional fiber-FSO-5G wireless convergent system. To compare with OFDM and OOK modulations, OFDM is less affected by the interferences than OOK, due to the data parallelization over several orthogonal subcarriers. Given that OOK modulation is feasible for the flexible bidirectional fiber-FSO-5G wireless convergent system, OFDM modulation is feasible for this proposed flexible bidirectional fiber-FSO-5G wireless convergent system as well due to better interference resilience.

IV. CONCLUSION

A flexible bidirectional fiber-FSO-5G wireless convergent system with downstream intensity-modulated 1-Gb/s/4.5-GHz (sub-6 GHz) and 10-Gb/s/28-GHz (MMW) 5G hybrid data signals, and an upstream phase-modulated 10-Gb/s/24-GHz 5G MMW data signal through a 25-km SMF transport, 600-m FSO link, and 10-m/4-m RF wireless transmission is successfully established. With a VCSEL-based wavelength selector to adaptively choose the desired 5G optical signal, the feasibility of

transmitting downstream 1-Gb/s/4.5-GHz sub-6 GHz or 10-Gb/s/28-GHz MMW 5G hybrid data signals is demonstrated. With a remotely injection-locked DFB LD to make a PM-to-IM transformation with an O/E conversion, the feasibility of delivering upstream 10-Gb/s/24-GHz 5G MMW data signal is developed. This demonstrated fiber-FSO-5G wireless convergent system is a promising convergence that meets the targets demanded by 5G communications. It opens up an innovative way for developing a flexible two-way high-speed and long-haul communication, due to its enhancement for integrating optical fiber with optical/5G wireless networks.

REFERENCES

[1] E. Garro et al., "5G mixed mode: NR multicast-broadcast services," IEEE Trans. Broadcast., vol. 66, no. 2, pp. 390–403, Jun. 2020.

[2] S. Henry, A. Alsohaily, and E. S. Sousa, "5G is real: Evaluating the compliance of the 3GPP 5G new radio system with the ITU IMT-2020 requirements," IEEE Access, vol. 8, pp. 42828–42840, Mar. 2020.

[3] I. Tomkos, D. Klonidis, E. Pikasis, and S. Theodoridis, "Toward the 6G network era: Opportunities and challenges," IEEE IT Prof., vol. 22, no. 1, pp. 34–38, Jan./Feb. 2020.

[4] Y. Yang, "Multi-tier computing networks for intelligent IoT," Nat. Electron., vol. 2, pp. 4–5, Jan. 2019.

[5] L. Huang et al., "Microwave photonic RF front-end for co-frequency co-time full duplex 5G communication with integrated RF signal self-interference cancellation, optoelectronic oscillator and frequency down-conversion," Opt. Express, vol. 27, no. 22, pp. 32147–32157, Oct. 2019.

[6] T. Kusunoki, T. Kurakake, K. Otsuki, and K. Saito, "Improvement of 4K/8K multi-channel IP multicast using DOCSIS over in-building coaxial cable network," in Proc. IEEE Intl. Conf. Consum. Electron. (ICCE), Jan. 2019, pp. 1–5.

[7] D. Fujimoto, H. H. Lu, K. Kumamoto, S. E. Tsai, Q. P. Huang, and J. Y. Xie, "Phase-modulated hybrid high-speed Internet/WiFi/Pre-5G in-building networks over SMF and PCF with GI-POF/IVLLC transport," IEEE Access, vol. 7, pp. 90620–90629, Jul. 2019.

[8] N. Eiselt et al., "Performance comparison of 112-Gb/s DMT, Nyquist PAM4, and partial-response PAM4 for future 5G Ethernet-based fronthaul architecture," IEEE/OSA J. Lightw. Technol., vol. 36, no. 10, pp. 1807–1814, May 2018.

[9] C. Y. Li, X. H. Huang, H. H. Lu, Y. C. Huang, Q. P. Huang, and S. C. Tu, "A WDM PAM4 FSO–UWOC integrated system with a channel capacity of 100 Gb/s," IEEE/OSA J. Lightw. Technol., vol. 38, no. 7, pp. 1766–1776, Apr. 2020.

[10] H. W. Wu et al., "A 448-Gb/s PAM4 FSO communication with polarization-multiplexing injection-locked VCSELs through 600 m free-space link," IEEE Access, vol. 8, pp. 28859–28866, Feb. 2020.

[11] W. G. Alheadary et al., "Free-space optical channel characterization and experimental validation in a coastal environment," Opt. Express, vol. 26, no. 6, pp. 6614–6628, Mar. 2018.

[12] W. C. Wang, H. Y. Wang, and G. R. Lin, "Ultrahigh-speed violet laser diode based free-space optical communication beyond 25 Gbit/s," Sci. Rep., vol. 8, Sep. 2018, Art. no. 13142.

[13] Y. W. Chen et al., "Asynchronous multi-service fiber-wireless integrated network using UFMC and PS for flexible 5G applications," in Proc. Opt. Fiber Commun. Conf. Exhib., Mar. 2020, pp. 1–3.

[14] Y. Zhao, W. Shi, H. Shi, W. Liu, Z. Wang, and J. Zhang, "Resource allocation for hybrid RF/FSO multi-channel multi-radio wireless mesh networks," IEEE Access, vol. 8, pp. 9358–9370, Jan. 2020.

[15] M. V. Jamali and H. Mahdavifar, "Uplink non-orthogonal multiple access over mixed RF-FSO systems," IEEE Trans. Wirel. Commun., vol. 19, no. 5, pp. 3558–3574, May. 2020.

[16] C. H. Yeh, W. P. Lin, C. M. Luo, Y. R. Xie, Y. J. Chang, and C. W. Chow, "Utilizing single lightwave for delivering baseband/FSO/MMW traffics simultaneously in PON architecture," IEEE Access, vol. 7, pp. 138927–138931, Oct. 2019.

[17] C. H. Chang, L. S. Tu, Y. S. Huang, and C. Y. Li, "Upgradable radio-over-fiber transport system," Opt. Eng., vol. 56, no. 10, Oct. 2017. Art. no. 106110.

[18] C. Y. Lin et al., "A full-duplex lightwave transmission system with an innovative VCSEL-based PM-to-IM converter," Opt. Express, vol. 22, no. 8, pp. 9993–10001, Apr. 2014.

[19] T. Mochii *et al.*, "A flexibly bidirectional wireless-over-fiber transport system," *IEEE Photon. J*, vol. 7, no. 6, Dec. 2015, Art. no. 7904409.

[20] S. Mechels, L. Muller, G. D. Morley, and D. Tillett, "1D MEMS-based wavelength switching subsystem," *IEEE Commun. Mag.*, vol. 29, no. 24, pp. 88–94, Mar. 2003.

[21] Y. Gao, Z. Tan, X. Chen, and G. Chen, "A hybrid algorithm for multi-beam steering of LCOS-based wavelength selective switch," *IEEE Photon. J.*, vol. 12, no. 3, Jun. 2020, Art. no. 7903011.

[22] C. Y. Chen *et al.*, "Bidirectional phased-modulated hybrid cable television/radio-over-fiber lightwave transport systems," *Opt. Lett.*, vol. 38, no. 4, pp. 404–406, Feb. 2013.

[23] W. Li, N. H. Zhu, L. X. Wang, and H. Wang, "Broadband phase-to-intensity modulation conversion for microwave photonics processing using Brillouin-assisted carrier phase shift," *IEEE/OSA J. Lightw. Technol.*, vol. 29, no. 24, pp. 3616–3621, Dec. 2011.

[24] C. Y. Li, H. W. Wu, H. H. Lu, W. S. Tsai, S. E. Tsai, and J. Y. Xie, "A hybrid internet/CATV/5G fiber-FSO integrated system with a triple-wavelength polarization multiplexing scenario," *IEEE Access*, vol. 7, pp. 151023–151033, Oct. 2020.

[25] H. K. Sung, E. K. Lau, and M. C. Wu, "Optical single sideband modulation using strong optical injection-locked semiconductor lasers," *IEEE Photon. Technol. Lett.*, vol. 19, no. 13, pp. 1005–1007, Jul. 2007.

[26] H. S. Ryu, Y. K. Seo, and W. Y. Choi, "Dispersion-tolerant transmission of 155-Mb/s data at 17 GHz using a 2.5-Gb/s-grade DFB laser with wavelength-selective gain from an FP laser diode," *IEEE Photon. Technol. Lett.*, vol. 16, no. 8, pp. 1942–1944, Aug. 2004.

[27] H. Kaushal and G. Kaddoum, "Optical communication in space: Challenges and mitigation techniques," *IEEE Commun. Surveys Tuts.*, vol. 19, no. 1, pp. 57–96, 2017.

[28] J. Zhang *et al.*, "Fiber–wireless integrated mobile backhaul network based on a hybrid millimeter-wave and free-space-optics architecture with an adaptive diversity combining technique," *Opt. Lett.*, vol. 41, no. 9, pp. 1909–1912, May 2016.

[29] L. C. Andrews and R. L. Phillips, *Laser Beam Propagation Through Random Media*, 2nd Ed., Bellingham, WA, USA: SPIE Press, 2005.

[30] I. I. Kim, B. McArthur, and E. Korevaar, "Comparison of laser beam propagation at 785 nm and 1550 nm in fog and haze for optical wireless communications," in *Proc. SPIE*, vol. 4214, pp. 26–37, Feb. 2001.

[31] Y. H. Lin *et al.*, "100-Gbit/s/λ EML transmitter and PIN-PD+TIA receiver-based inter-data center link," *IEEE/OSA J. Lightw. Technol.*, vol. 38, no. 8, pp. 2144–2151, Apr. 2020.

[32] S. A. K. Tanoli *et al.*, "Impact of relay location of STANC bi-directional transmission for future autonomous internet of things applications," *IEEE Access*, vol. 8, pp. 29395–29406, Feb. 2020.

[33] A. Upadhya, V. K. Dwivedi, and G. K. Karagiannidis, "On the effect of interference and misalignment error in mixed RF/FSO systems over generalized fading channels," *IEEE Trans. Commun.*, vol. 68, no. 6, pp. 3681–3695, Jun. 2020.

[34] 2020. [Online]. Available: http://www.voscom.com/trainning/fiber-optic-dispersion.asp

[35] A. D. Ellis, M. E. Mccarthy, M. A. Z. AL Khateeb, M. Sorokian, and N. J. Doran, "Performance limits in optical communications due to fiber nonlinearity," *Adv. Opt. Photon.*, vol. 9, no. 3, pp. 429–503, Sep. 2017.

[36] P. Saboureau, J. P. Foing, and P. Schanne, "Injection-locked semiconductor lasers with delayed optoelectronic feedback," *IEEE J. Quantum Electron.*, vol. 33, no. 9, pp. 1582–1591, Sep. 1997.

[37] Q. Gu, W. Hofmann, M. C. Amann, and L. Chrostowski, "Optically injection-locked VCSEL as a duplex transmitter/receiver," *IEEE Photon. Technol. Lett.*, vol. 20, no. 7, pp. 463–465, Apr. 2008.

[38] E. I. Ackerman, C. Cox, III, G. Betts, H. Roussell, K. Ray, and F. O'Donnell, "Input impedance conditions for minimizing the noise figure of an analog optical link," *IEEE Trans. Microw. Theory Tech.*, vol. 46, no. 12, pp. 2025–2031, Dec. 1998.

Chung-Yi Li received the M.S. and Ph.D. degrees from the Department of Electro-Optical Engineering, National Taipei University of Technology (NTUT), Taiwan, in 2008 and 2012, respectively. From 2013 to 2014, he was an Engineer with the Innovation and Product Development Department, FOCI Fiber Optic Communications Inc., Hsinchu, Taiwan. He joined the Department of Electro-Optical Engineering with NTUT as a Research Assistant Professor in 2014. He then joined the Department of Communication Engineering, National Taipei University as an Assistant Professor in 2018. His research interests include FSO communications, fiber-wireless convergence, and fiber-FSO convergence.

Hai-Han Lu (Senior Member, IEEE) received the M.S. and Ph.D. degrees from the Institute of Optical Science, National Central University, Taiwan, in 1991 and 2000, respectively. He joined the Department of Electro-Optical Engineering, National Taipei University of Technology (NTUT) as an Associate Professor in 2003. He was promoted to a Professor, Distinguished Professor, and to a Lifetime Distinguished Professor in 2003, 2006, and 2017, respectively. He has authored or coauthored more than 200 papers in SCI-cited international journals and more than 130 papers in international conferences. His research interests include FSO communications, fiber-FSO convergence, UWOC systems, and FSO-UWOC integration. Professor Lu is currently a Fellow of SPIE, a Fellow of IET, and a Senior Member of OSA. He was awarded with the Sun Yat-Sen Academic Award (Natural Science, 2017), National Invention Award (Gold Medal, 2016), ICT Month Innovative Elite Products Award (2014 and 2016), Outstanding Electrical Engineering Professor Award of the Chinese Institute of Engineering (2015), Outstanding Engineering Professor Award of the Chinese Engineer Association (2013), and Outstanding Research Award of NTUT (2004) for his significant technical contributions to FSO communications, fiber-FSO convergence, fiber-wireless convergence, and fiber-FSO-wireless convergent systems.

Ching-Ru Chou was born in Taoyuan city, Taiwan, in June 1997. He received the B.S. degree from Yuan Ze University, Taoyuan, Taiwan, in 2019. He is currently working toward the M.S. degree with the Institute of Electro-Optical Engineering, National Taipei University of Technology, Taiwan. His research interests focus on FSO communications and fiber-FSO convergence.

Hsin-Mao Hsia was born in Hsinchu, Taiwan, in November 1995. He received the B.S. degree from Tunghai University, Taichung, Taiwan, in 2019. He is currently working toward the M.S. degree with the Institute of Electro-Optical Engineering, National Taipei University of Technology, Taiwan. His research interests focus on FSO communications and fiber-wireless convergence.

Chao-Yu Feng was born in Tainan, Taiwan, in December 1995. He received the B.S. degree from the National Kaohsiung University of Science and Technology, Kaohsiung, Taiwan, in 2019. He is currently working toward the M.S. degree with the Institute of Electro-Optical Engineering, National Taipei University of Technology, Taiwan. His research interests focus on FSO communications.

Yi-Hao Chen was born in Changhua County, Taiwan, in March 1997. He received the B.S. degree from the National Yunlin University of Science and Technology, Yunlin County, Taiwan, in 2019. He is currently working toward the M.S. degree with the Institute of Electro-Optical Engineering, National Taipei University of Technology, Taiwan. His research interests focus on FSO communications and fiber-wireless convergence.

Yu-Ting Huang was born in Yilan, Taiwan, in August 1995. She received the B.S. degree from the Minghsin University of Science and Technology, Hsinchu, Taiwan, in 2018. She is currently working toward the M.S. degree with the Institute of Electro-Optical Engineering, National Taipei University of Technology, Taiwan. Her research interests focus on FSO communications and fiber-wireless convergence.

Agustina Nainggolan was born in Medan, Indonesia, in August 1996. She received the B.S. degree from the University of North Sumatra, Medan, Indonesia, in 2018. She is currently working toward the M.S. degree with the Department of Electrical Engineering and Computer Science, National Taipei University of Technology, Taiwan. Her research interests focus on FSO communications and fiber-FSO convergence.